Microshock wave propagation in molecular clusters

Israel Schek and Joshua Jortner
The Raymond and Beverly Sackler Faculty of Exact Sciences, School of Chemistry, Tel Aviv University, Ramat Aviv, 69978 Tel Aviv, Israel

(Received 16 October 1995; accepted 17 November 1995)

Microshock wave propagation in Ar_N ($N=55$–555) clusters generated by high-energy cluster-Pt surface impact (cluster velocities $v=1$–10 km s^{-1}) is explored by molecular dynamics simulations. The gross features of the dynamics of the intracluster microshock wave propagation at this impact velocity range are not sensitive to the details of the repulsive potential (i.e., the Lennard-Jones or the exp-6 form). The propagation of the microshock within the cluster was quantified by the time dependence of the first moment of the total energy. A linear dependence between the microshock (compression) velocity u_s and the cluster impact velocity v is observed and for sufficiently large clusters ($N \geqslant 321$) $u_s \approx v$. For large clusters ($N>321$), the cluster Hugoniot temperature–pressure relations are qualitatively similar to those for the compression of macroscopic fluid Ar. © *1996 American Institute of Physics.* [S0021-9606(96)02908-4]

I. INTRODUCTION

High-energy impact of atomic or molecular cluster ions (of sizes of 10–1000 constituents, with velocities up to ~20 km s^{-1} and kinetic energies up to ~100 eV per particle) on insulator, semiconductor or metal surfaces,[1–32] produces a new medium of extremely high density (up to ~4 times the standard density),[1–3] high temperature (up to ~10^5 K),[26–28] and high energy density (up to 10^2 eV per particle),[26–28] which is temporarily generated during the propagation of a microshock wave within the cluster on the 10^2–10^3 fs time scale.[1–3,26–28] Experimental studies of electron emission,[23–25] surface coating,[11–15] molecular dissociation,[28–32] and fragmentation[18–22] induced by high-energy cluster–wall collisions, provide information on some unique homogeneous and heterogeneous processes of energy acquisition and disposal, which occur on the ultrashort time scale of vibrational molecular motion. Some attempts to provide a microscopic description of the intracluster shock wave[29–31] and of cluster-impact chemistry[13–15,29–32] rested on molecular dynamics simulations of high-energy collisions of inert gas clusters with ionic[26,33] and metallic[27–31] surfaces and of metal clusters with metallic surfaces.[11–15] Another approach was based on the use of the equations of state for the macroscopic material for deuterium clusters,[1–3] and on the use of the continuum matter description for the mechanical compression stress in copper clusters.[26,33] Of considerable interest is microshock wave propagation in clusters, which constitutes the response of a finite system to extremely high pressure changes. The description of the mechanical properties of clusters under extreme conditions of cluster–wall collisions is of interest because of the following reasons:

(1) The characterization of the microshock wave in a finite system, e.g., the propagation velocity, temperature, energy, and pressure.
(2) The description of the equations of state of a finite system under the extreme conditions of temperature and pressure.
(3) The microscopic analog of the Hugoniot equations.[34–36] These are provided by the relations between the microshock velocity and the intensive thermodynamic variables.
(4) Cluster size effects on shock propagation in finite systems and their evolution towards the mechanical properties of the bulk[34–36] with increasing the cluster size.
(5) The high-energy acquisition processes in clusters, which trigger energy-impact chemical processes.

In this paper we address the propagation of the microshock wave within Ar_N clusters ($N=55$–555) colliding ($v=2$–10 km s^{-1}) with a realistic Pt surface, as explored by molecular dynamics simulations.

II. METHODOLOGY

A. Molecular dynamics simulations

Our molecular dynamics (MD) simulations procedures for high-energy collisions of Ar_N ($N=55$–555) clusters ($T=10$ K and center of mass velocities $v=1$–10 km s^{-1}) with a realistic Pt surface (720 atoms) arranged in six layers of 120 atoms each, were previously described.[27] The potential for the Pt surface was represented as before[28,29,31] by a many-body Gupta potential[37] based on the Friedel model for d-electron transition metals.[38] To account for the interaction with the metal bulk, we have imposed a thermalization condition on the interior of the surface metal atoms, which are coupled to a heat bath with the bulk temperature $T=300$ K.[28]

B. Potentials

Two sets of potentials for the Ar–Ar and Ar–Pt atom–atom interactions were utilized.

(i) Lennard-Jones (LJ) pair potentials. These involved Ar–Ar potentials[39] and Ar–Pt potentials extracted for Ar scattering from a Pt surface. The potential parameters were $\epsilon_{Ar-Ar}=1.044\times10^{-2}$ eV, $\sigma_{Ar-Ar}=3.40$ Å, $\epsilon_{Ar-Pt}=5.18\times10^{-3}$ eV, $\sigma_{Ar-Pt}=4.01$ Å. This traditional empirical form of the potential is intrinsically limited at high densities, prevailing for microshock

propagation, where the empirical inverse twelfth power of the repulsive potential is unrealistic.

(ii) The Ar–Ar exp-6 pair potential[40] is

$$v(r)=\epsilon\left\{\left(\frac{6}{\alpha-6}\right)\exp[\alpha(1-r/r_m)]-\left(\frac{\alpha}{\alpha-6}\right)\left(\frac{r_m}{r}\right)^6\right\}. \tag{1}$$

The exp-6 potential parameters for Ar–Ar were chosen as $\epsilon=1.19\times10^{-2}$ eV, $r_m=3.77$ Å, and $\alpha=14.8$, which constitute mean values between those given by Sherwood and Prausnitz ($\epsilon=152.02$ K, $r_m=3.644$ Å, $\alpha=18$) (Ref. 41) and Ross and Radousky ($\epsilon=122$ K, $r_m=3.85$, $\alpha=13.2$).[42] The exp-6 potential parameters for Ar–Pt were taken to be identical to those for Ar–Xe,[43] i.e., $\epsilon=1.50\times10^{-2}$ eV, $r_m=4.13$ Å, and $\alpha=14.8$. These exp-6 potential parameters provide a useful semiempirical potential, which provides a reasonable description of the repulsive potential stiffness.

C. Adiabatic dynamics

Our dynamics MD simulations are restricted to the dynamics on the ground electronic potential surface. The role of the electronic excitations of the Ar_N cluster is expected to be unimportant provided that the total (potential and kinetic) intracluster energy (per pair of atoms) does not exceed the electronic cluster excitation energy. These nonvertical excitation energies are approximated by the lowest crossings of the potential curves of the ground state and of the lowest electronically excited state. These curve crossings between $Ar(^1S_0)+Ar(^1S_0)$ and $Ar(^1S_0)+Ar(^3P_1)$ are exhibited in the repulsive range of both the ground state and the electronically excited potential curves. The lowest electronic excitation of the Ar_N cluster corresponds to the $Ar_2^*(^3\Sigma_u)$ excimer[44] with the nonvertical electronic excitation (above the minimum of the ground state of Ar_2) being >13 eV.[44] Provided that specific high-energy pair interactions[44] are neglected, a necessary condition for ground state adiabatic dynamics is $YE_K/N<13$ eV, where $Y\cong0.5$ is the yield of energy deposition into the cluster[27] and E_K is the cluster impact kinetic energy. Thus $E_K/N<26$ eV, which corresponds to cluster center-of-mass velocity $v<10$ km s^{-1}. We shall consider the cluster impact velocity $v<10$ km s^{-1} as the upper limit for the absence of the interesting effects of electronic excitations and restrict our analysis to this domain, performing MD simulations for Ar_N ($N=55$–555) cluster impact on a Pt surface for $v=1$–10 km s^{-1}.

III. ENERGY ACQUISITION

To quantify the energy acquisition process by the cluster and by the surface, we present in Fig. 1 the temporal evolution of the cluster potential energy (CPE), the cluster temperature (T_c) and the cluster–surface interaction energy (CSI) for Ar_{555} and Ar_{55} clusters colliding with a Pt wall at $v=5$–10 km s^{-1}. The simulations were performed using both the LJ potentials (i) and the exp-6 potential (ii). For each simulation the results by 20 trajectories were averaged with the equilibrated cluster being initially oriented at random Euler angles with respect to the surface. The characteristics of the cluster–wall collisions (Fig. 1) are manifested[27–31] by

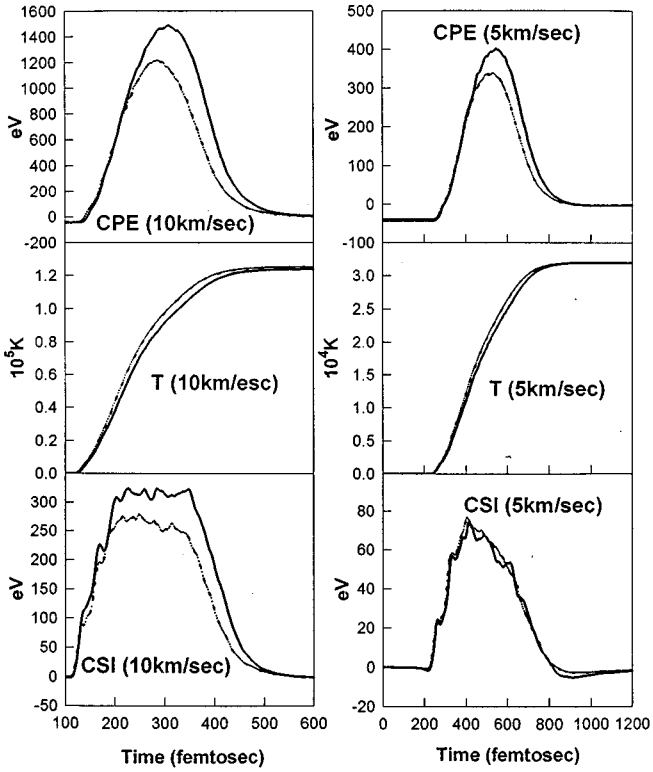

FIG. 1. Comparison of the time evolution of the cluster potential energy (CPE), the cluster temperature (T), and the cluster–surface interaction (CSI) of an Ar_{555} cluster at two impact velocities [$v=10$ km s^{-1} (left) and 5 km s^{-1} (right), respectively] for two potential models; the exponent-6 (full line) and the Lennard-Jones (dashed line).

(1) the impact onset at the time thresholds τ_0 of the (temporally coincident) rises of CPE, T_c and CSI;
(2) the (nearly temporally coinciding) maxima of CPE and CSI;
(3) the increase of T_c to saturation at a high value;
(4) the cluster residence time τ given by the width (FWHM) of the CPE curve which is close to FWHM of the CSI curve;
(5) the time τ_M corresponding to the maximum of the CPE, which gives the time scale $\tau_{CEA}=\tau_M-\tau_0$ for the maximum of the CPE, signifying the time for the intracluster energy acquisition.

From the technical point of view we note that in this velocity domain $v<10$ km s^{-1} ($E_K/N<26$ eV) the dynamic observables for energy acquisition, i.e., the time dependence of CPE, T_c and CSI calculated using the LJ (i) and the exp-6 (ii) pair potentials, do not differ by more than 20%. At relatively short times above τ_0, i.e., $\tau_0\leqslant t\leqslant\tau/2$, the time dependence of CPE, T_c and CSI calculated using the potentials (i) and (ii) is practically identical, while for longer times, i.e., $t>\tau/2$ and in the vicinity of $t\cong\tau$ the dynamic observables calculated with the Ar–Ar exp-6 potential are higher by about 20% than those calculated with the LJ potential (Fig.

TABLE I. Characteristic time τ^a and $\tau_{CEA}{}^b$ for cluster–Pt wall impact.

	LJ potential		exp-6 potential	
v (km s^{-1})	τ (fs)	τ_{CEA} (fs)	τ (fs)	τ_{CEA} (fs)
5	292	259	324	292
10	169	162	182	182

[a] τ is the cluster residence time.
[b] τ_{CEA} is the time for the maximum of the CPE.

1). The characteristic times τ and τ_{CEA} calculated with the LJ and exp-6 potentials show a variance of ~10% (Table I). Just above the onset of the propagation of the microshock wave the dynamics of the energy acquisition is practically invariant with respect to the form of the repulsive potential, while for longer times the dynamic observables exhibit only a moderate (~10%–20%) variation with respect to the form of the repulsive potential. We conclude that for the relevant cluster impact velocity range $v \leqslant 10$ km s^{-1}, which is of interest to us, where electronic excitations can be neglected (Sec. II C), the gross features of the dynamics of the intracluster microshock propagation are not sensitive to the details of the repulsive potential, i.e., the LJ or the exp-6 form. This analysis provides a justification for our previous use of the LJ potentials for the description of cluster–wall collisions in this impact velocity domain.[27,28] For higher cluster impact velocities ($v > 10$ km s^{-1}) we expect larger deviations between the simulation results, which are based on the LJ and the exp-6 potential parameters. On the basis of extensive simulation results for shock wave compression curves in macroscopic fluid Ar reported by Ross,[35,45–50] one expects that in the high pressure domain the exp-6 pair potential should be preferred. For our simulations of microshock propagation in inert-gas clusters ($v \leqslant 10$ km s^{-1}) either the LJ or the exp-6 potentials are adequate. In what follows we shall utilize the exp-6 potentials, Eq. (1), for the characterization of the propagation of intracluster microshock wave generated by the impact of Ar_N clusters on a Pt surface.

IV. THE INTRACLUSTER MICROSHOCK WAVE

The impact excited cluster constitutes a finite system under extreme conditions of temperature and pressure. The cluster temperatures $k_B T_c =$ (cluster kinetic energy)/[3/2($N-6$)] for $v = 1$–10 km s^{-1} (at times corresponding to the maximum of CPE) are remarkably high, reaching the value of $T_c = 1.2 \times 10^5$ K for $E_K/N = 21$ eV (Fig. 2). As $k_B T_c$ is considerably lower than the horizontal excitation energy of the Ar($^3P_1$) atom or of the Ar_2^* excimer (13 eV according to Sec. II), we obtain an *a posteriori* justification for neglecting electronic excitations. T_c increases linearly with increasing E_K (Fig. 2) being of the form $T_c = \alpha(E_K/N)$ with $\alpha = (5 \pm 0.5)\ 10^3$ eV^{-1} K, being independent of the cluster size for $E_K/N = 0.2$–22 eV.

To explore the microshock propagation within the cluster, we conducted cluster space slicing, in analogy to continuous matter studies.[34] Since the present problem is characterized by cylindrical symmetry (with the symmetry axis being perpendicular to the surface, along the impact velocity direction) the cluster is divided into slices parallel to the surface, each slice containing 1–3 atom layers (Fig. 3), i.e., the number of atoms in each slice being 10–40. The total energy of each slice is then calculated. Figure 3 shows a typical correlation between the internal energy (kinetic +potential energy) of the slices and the distances of these slices from the metal surface, which is obtained for various time snapshots. The origin of the time scale is taken as $\tau_0 = 0$. At the time preceding the cluster–surface collisions ($t < 0$) the (low) energy is uniformly spread within the cluster (Fig. 3). Subsequent to cluster–surface impact, high energy accumulates in the cluster spatial region close to the surface (Fig. 3). Prior to the collision (Fig. 3, first frame, $t = -10$ fs), the energy profile of the cluster reflects the fact that the spherical cluster is sliced by parallel surfaces, where the central slice contains the largest number of atoms (30–40 atoms), corresponding to a minimum of the energy. After the collision, the high energy domain spreads into the interior slices (Fig. 3), manifesting the propagation of the microshock wave within the cluster during the cluster contraction. At times prior to the maximum of the CPE, i.e., $t < \tau_{CEA}$ and $t < \tau$ (e.g., up to ~200 fs for Ar_{555} at an impact velocity $v = 10$ km s^{-1}) the compression shock wave runs forward into the cluster, manifesting a single wave (left column in Fig. 3). At longer times, i.e., $t > \tau_{CEA}, \tau$, a secondary backward shock wave piles up, being close to the Pt surface and running towards it. Subsequently the primary (forward) and the secondary (backward) shock waves disjoint locally (at $t > 280$ fs for Ar_{555} at $v = 10$ km s^{-1}, Fig. 3). Later, tertiary and higher order shock waves are generated due to the collision of the corresponding lower order shock waves with the surface. The propagation and

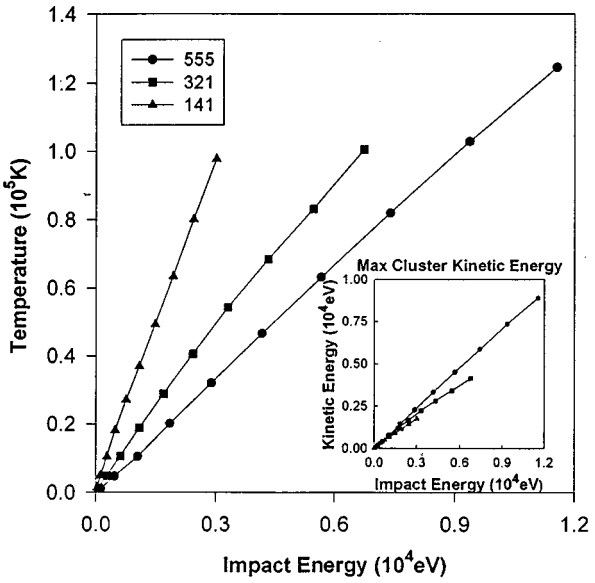

FIG. 2. Maximum temperature of Ar_N clusters ($N = 141,321,555$) colliding with the Pt surface for various impact energies. The inset shows the respective maximum cluster kinetic energies.

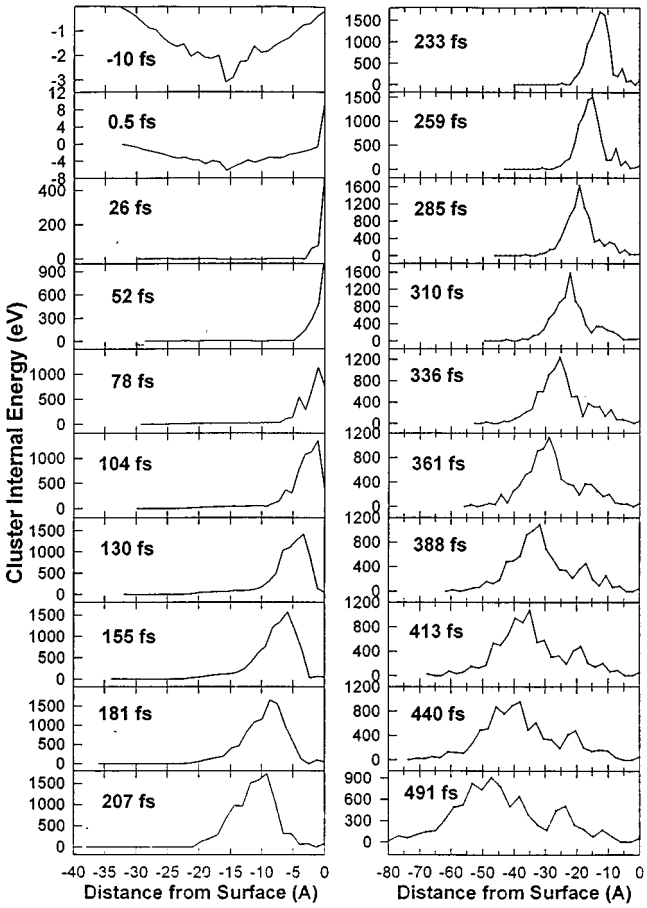

FIG. 3. Snapshots of the internal energy profile of an Ar_{555} cluster colliding with a Pt surface at an impact velocity $v=10$ km s^{-1}, at times prior to the collision, during the collision, and beyond the residence period (-10 fs$<t<\sim$500 fs). The time origin $t=0$ corresponds to the threshold of the rise of the CPE.

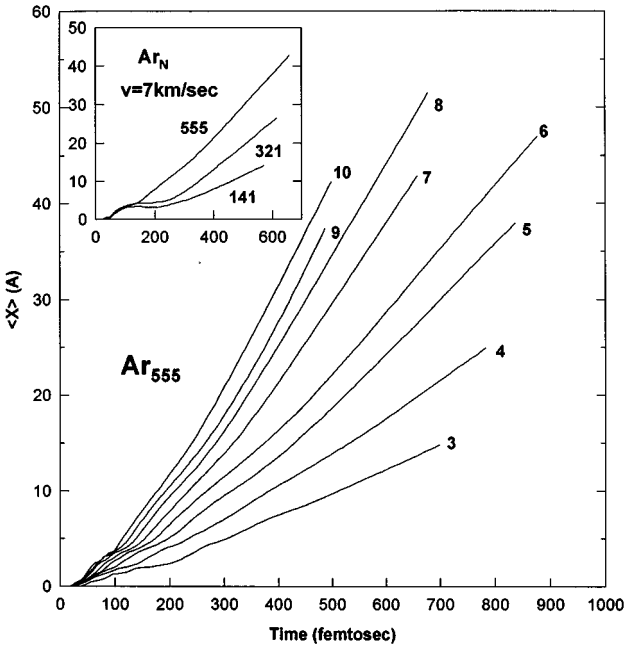

FIG. 4. The time dependence of the first moment $\langle X\rangle$ of the cluster total energy. $\langle X\rangle$ values, Eq. (2), were calculated by a numerical integration [for $E(X)\geqslant 0$] of the total energy profiles at fixed t. The main frame presents the data for Ar_{555} at $v=3$–10 km s^{-1}, where the numbers on the individual lines represent the values of v (km s^{-1}). The insert shows the data for Ar_N ($N=555,321,141$, which are marked on the lines) for $v=7$ km s^{-1}.

surface reflections of these higher order shock waves result in the disintegration of the cluster.

We quantified the microshock propagation within a cluster by defining the first moment $\langle X\rangle$ of the cluster energy,

$$\langle X\rangle=\int_0^\infty dXXE(X)\ \Big/\ \int_0^\infty dXE(X), \tag{2}$$

where $E(X)$ is the local energy at X. From the data of Fig. 4 we infer that the time dependence of $\langle X\rangle$ is nearly linear over a broad time domain for $N=555$, 321, and 141 in the impact velocity range $v=1$–10 km s^{-1}. The microshock wave propagation velocity u_s was determined from the linear time dependence of $\langle X\rangle$ (Fig. 4). Figure 5 shows the dependence of u_s on the cluster impact velocity v for Ar_N ($N=141$, 321, and 555) clusters. The u_s vs v dependence is linear (Fig. 5), being of the form $u_s=\eta v$. From Fig. 5 we obtain the slopes $\eta=0.39\pm0.05$ for $N=141$, $\eta=0.95\pm0.1$ for $N=321$, and $\eta=1.15\pm0.15$ for $N=555$.

Of considerable interest is the quantification of the propagation velocity of the microshock wave during the cluster contraction. From the foregoing analysis we conclude that for sufficiently large clusters, i.e., $N\geqslant 321$, $u_s/v=1.0\pm0.15$, with the velocity of the microshock wave propagation being close to the cluster impact velocity. This estimate for the propagation velocity of the microshock wave within a large cluster can be confronted with the results of the theory for shock compression in a macroscopic material.[34,35] For a

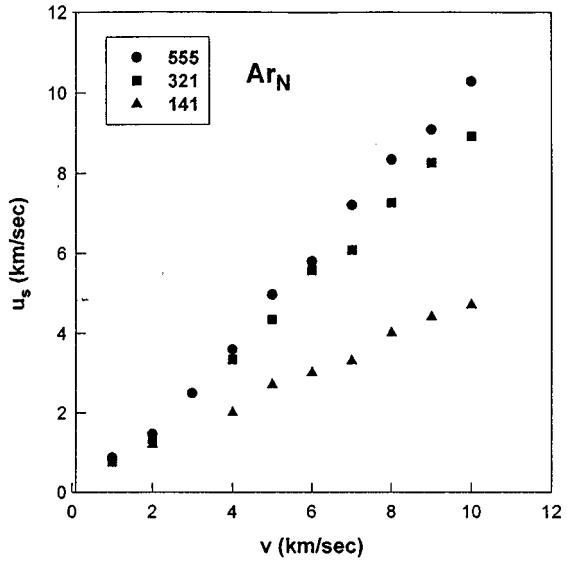

FIG. 5. The dependence of the shock velocity running in Ar_N clusters ($N=141,321,555$) on the cluster impact velocity, as obtained by analysis of the temporal evolution of energy profiles (shown in Fig. 3). Note the linear dependence for the larger clusters ($N=321,555$).

one-dimensional shock propagation at the velocity U_s, which is induced by a piston moving with the velocity U_p within the macroscopic material at thermodynamic equilibrium,[35,36] the conservation of mass, momentum and energy leads to the Hugoniot equations.[34,35] Mass conservation results in the relation between the shock velocity and the piston velocity in the form[35,36] $U_p/U_s=1-\rho_0/\rho_1$, where ρ_1 is the final (postshock) density during the shock wave. Attempting a heuristic bridging between shock propagation in the cluster and in the bulk, we identify the cluster impact velocity with the piston velocity, i.e., $U_p \cong v$, and the velocity of the inward propagation of the microshock wave within the cluster with the shock propagation velocity in a macroscopic material, i.e., $U_s \equiv u_s$. We also bear in mind that $\rho_0/\rho_1 \ll 1$. Accordingly, we expect that $U_p/U_s \cong v/u_s \cong 1$. This conclusion concurs with our results of the interrogation of the propagation of the microshock wave front within the large cluster.

To explore further the nature of large finite systems under extreme conditions of microshock propagation we estimate the pressure–temperature relations for the impact excited cluster. For a macroscopic material the Hugoniot equations result in the following relation for the pressure rise $p=p_0+[2U_s(E-E_0)]^{1/2}$, where p_0 is the initial (prior to collision) pressure, E_0 is the initial internal energy, while p is the pressure and E is the internal energy during the propagation of the shock wave. We have characterized the shock propagation at the time τ_{CEA}, which corresponds to the maximum of the CPE (Sec. III). Identifying u_s with U_s and bearing in mind that p_0 is negligible, we have utilized the heuristic relation $p=[2u_s(E-E_0)]^{1/2} \cong [2\eta v(E-E_0)]^{1/2}$ to calculate the relation between the internal energy rise, the shock velocity and the pressure rise. For Ar_{555} clusters two sets of $p-T_c$ data are presented. (1) Data at the maximum value of the CPE ($t=\tau_{\mathrm{CEA}}$), where the cluster already starts to expand and consequently to disintegrate. (2) Data at the half maximum of the CPE ($t=\tau_{\mathrm{CEA}}/2$), where the microshock wave is still heading into the cluster, and the reflected shock wave does not interfere. Figure 6 presents the micro Hugoniot curves for the $p-T_c$ relation for Ar_N ($N=141,321,555$) clusters at impact velocities $v=1-6$ km s^{-1}. It is interesting to confront the $p-T_c$ relations for the Ar_N finite clusters with the corresponding experimental and simulated shock compression data for macroscopic fluid.[45–50] The macroscopic liquid Ar Hugoniot shock wave $p-T$ data adopted from the results of Ross *et al.*[36,49,50] and reproduced in Fig. 6 reveal a similar slope to that obtained herein for the finite clusters, although the absolute values of p at a fixed T_c (for $t=\tau_{\mathrm{CEA}}$) are lower than the corresponding values of p at the same temperature for the macrosystem. We note in passing that the data for the microshock wave in Ar_{555} at $t=\tau_{\mathrm{CEA}}/2$ fit better the macroscopic adiabate. The present data are insufficient to provide a quantitative description for the cluster size effect of the mechanical properties under extreme conditions of temperature and pressure. At present we conclude that the $p-T_c$ relations for sufficiently large clusters ($N>300$) are qualitatively similar to those of the corresponding macroscopic material.

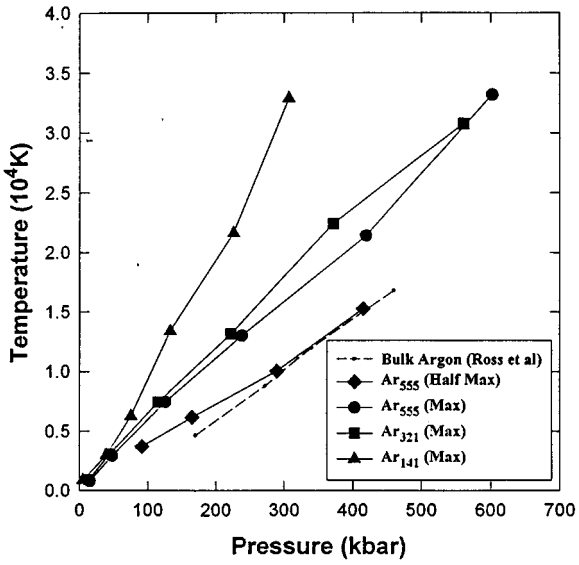

FIG. 6. Micro Hugoniot (pressure–temperature) adiabates for Ar_N clusters ($N=141,321,555$) at impact velocities $v=1-6$ km s^{-1}, at the maximum values of the CPE. For Ar_{555} clusters we also present the $T-P$ relation with the data calculated at $t=\tau_{\mathrm{CEA}}/2$ (marked Half Max). These molecular dynamics results are confronted with measurements of macroscopic fluid Ar compression (M. Ross *et al.*, Refs. 36, 49, 50).

A large finite cluster or an infinite system may be treated as a continuous medium when the mean free path prior to the shock wave generation is shorter than other physical dimensions.[51] The interatomic collision cross section in Ar clusters or bulk is $\sigma=\pi r_0^2 \cong 45$ Å^2, where $r_0 \cong 3.77$ Å is the interatomic distance estimate from the exp-6 potential parameters. Consequently, the mean free path $\lambda=(\sigma\rho_0)^{-1} \approx 0.74$ Å, where $\rho_0=3\times10^{22}$ cm^{-3}. As is evident from Fig. 3 the microshock wave front thickness l_s spreads over a distance $l_s \sim 5-8$ Å, which corresponds to $\sim 2r_0$. Accordingly $\lambda \ll l_s$, whereupon the internal shock structure can be disregarded and the present treatment of the continuum model description seems to be justified.

V. CONCLUDING REMARKS

The study of microshock propagation in molecular clusters is of considerable interest for the exploration of large finite systems under extreme thermodynamic conditions. High energy cluster–surface impact provides a novel medium for the investigation of ultrashort thermally driven reactions under extreme conditions of temperature and pressure.[28–31] In this context, the propagation of the microshock wave within the large cluster can be interrogated by a chemical probe, i.e., the homogeneous dissociation of a guest molecule in the cluster.[28–32] The velocity of the propagation of the dissociation front in doped I_2Ar_N clusters was found[31] to be close to the cluster impact velocity, in accord with the present results for the microshock wave propagation velocity in neat Ar_N clusters. On the experimental front, the consequences of microshock wave generation in neat molecular clusters, which result in extreme densities, pressures, and temperatures, can be interrogated by the measurements

of infrared or Raman spectra of neat clusters of polyatomic molecules [e.g., $(CO_2)_N$ or $(NH_3)_N$] or of a spectroscopic probe embedded in a cluster [e.g., SF_6Ar_N or $SF_6(CO_2)_N$]. The propagation of the microshock wave front can presumably be experimentally interrogated by femtosecond infrared or/and Raman spectroscopy of mixed molecular clusters with the impurity molecule being located in the cluster center, e.g., $SF_6(CO_2)_N$, or $I_2^-(CO_2)_N$.[32] The delay between the change of the spectrum of the host molecule due to the onset of the cluster–wall collision and the change of the guest molecule spectrum, will provide a clue for the propagation of the microshock wave within the cluster.

Finally, we would like to point out that another fascinating aspect of microshock waves in finite systems pertains to the possibility of compression of nuclear matter in high-energy nucleus–nucleus collisions,[52,53] which are expected to bear a close analogy, i.e., high densities and high temperatures, to cluster–wall collisions.

ACKNOWLEDGMENTS

We are grateful to Professor R. D. Levine, Professor K. L. Kompa, Professor Y. M. Eisenberg, and Professor B. Svetitsky for useful discussions. This research was supported by the German–Israel Binational James Franck Program on laser–matter interactions.

[1] R. J. Beuhler and L. Friedman, Int. J. Mass Spectrom. Ion Phys. **81**, 23 (1977).
[2] L. Friedman and G. H. Vineyard, Comments At. Mol. Phys. **51**, 251 (1977).
[3] R. J. Beuhler and L. Friedman, Chem. Rev. **86**, 521 (1986).
[4] M. H. Shapiro and T. A. Tombrello, Phys. Rev. Lett. **65**, 92 (1990).
[5] M. H. Shapiro and T. A. Tombrello, Phys. Rev. Lett. **68**, 1613 (1992).
[6] Y. Yamamura, Nucl. Instrum. Methods Phys. Res. B **45**, 707 (1990).
[7] J. F. Mahony, J. Perel, T. D. Lee, P. A. Martino, and P. Williams, J. Am. Soc. Mass Spectrom. **3**, 311 (1992).
[8] P. R. Wolfgang and R. Klingelhöfner, J. Phys. C **2**, 159 (1989).
[9] V. I. Shulga, Nucl. Instrum. Methods Phys. Res. B **58**, 422 (1991).
[10] H. Hsie, R. S. Averbach, H. Sellers, and C. P. Flynn, Phys. Rev. B **45**, 4417 (1992).
[11] H. Haberland, M. Karraris, M. Mall, and Y. Thurner, J. Vac. Sci. Technol. A **10**, 3266 (1992).
[12] H. Haberland, Z. Insepov, and M. Moseler, Z. Phys. D **26**, 229 (1993).
[13] I. Yamada, G. H. Takaoka, H. Usui, and S. K. Koh, Mater. Res. Soc. Symp. Proc. **206**, 383 (1991).
[14] I. Yamada, Appl. Surf. Sci. **43**, 23 (1989).
[15] Y. Yamamura, I. Yamada, and T. Tagaki, Nucl. Instrum. Methods B **37/38**, 902 (1987).
[16] K. H. Müller, J. Appl. Phys. **61**, 2516 (1987).
[17] H. P. Cheng and U. Landman, J. Phys. Chem. **98**, 3527 (1994).
[18] P. M. St. John, R. D. Beck, and R. L. Whetten, Phys. Rev. Lett. **69**, 1467 (1992).
[19] P. M. St. John and R. L. Whetten, Chem. Phys. Lett. **196**, 330 (1992).
[20] R. D. Beck, P. M. St. John, M. M. Alvarez, F. Dietrich, and R. L. Whetten, J. Phys. Chem. **95**, 8402 (1991).
[21] C. Yeretzian and R. L. Whetten, Z. Phys. D **24**, 199 (1992).
[22] C. Yeretzian, K. Hansen, and R. L. Whetten, Science **260**, 652 (1993).
[23] U. Even, P. de Lange, H. Jonkman, and J. Kommandeur, Phys. Rev. Lett. **56**, 956 (1986).
[24] H. Kunz, H. Winter, P. Scheier, and T. D. Märk, Europhys. Lett. **22**, 297 (1993).
[25] U. Even and E. Hendell, J. Chem. Phys. (in press).
[26] C. L. Cleveland and U. Landman, Science **257**, 355 (1992).
[27] U. Even, I. Schek, and J. Jortner, Chem. Phys. Lett. **202**, 303 (1993).
[28] I. Schek, T. Raz, R. D. Levine, and J. Jortner, J. Chem. Phys. **101**, 8566 (1994).
[29] T. Raz, I. Schek, M. Ben Nun, U. Even, J. Jortner, and R. D. Levine, J. Chem. Phys. **101**, 8606 (1994).
[30] T. Raz and R. D. Levine, J. Am. Chem. Soc. **116**, 11 167 (1994).
[31] (a) T. Raz, R. D. Levine, I. Schek, and J. Jortner, Proceedings of the Yamada Conference (in press); (b) I. Schek, J. Jortner, T. Raz, and R. D. Levine, Chem. Phys. Lett. (submitted).
[32] H. Yamamatsu, T. Tsukuda, T. Sugai, A. Terasaki, T. Nataga, and T. Kondow, Surf. Sci. Lett. (in press).
[33] D. Scharf, U. Landman, and J. Jortner, J. Chem. Phys. **88**, 4273 (1988).
[34] Ya. B. Zeldovich and Yu, P. Raizer, *Physics of Shock Waves and High Temperature Hydrodynamics Phenomena* (Academic, New York, 1979).
[35] M. Ross, J. Chem. Phys. **71**, 1567 (1979).
[36] M. Ross, in *High Pressure Chemistry and Biochemistry*, edited by R. van Eldik and J. Jonas (Reidel, New York, 1987).
[37] R. Gupta, Phys. Rev. B **23**, 6265 (1981).
[38] J. Friedel, in *The Physics of Metals*, edited by J. M. Ziman (Cambridge University, Cambridge, 1969).
[39] G. Vidali, G. Ihm, H. Y. Kim, and M. W. Cole, Surf. Sci. Rep. **12**, 133 (1991).
[40] J. A. Barker, in *Rare Gas Solids*, edited by M. L. Klein and J. A. Venables (Academic, London, 1976), Vol. 1.
[41] A. E. Sherwood and J. M. Prausnitz, J. Chem. Phys. **41**, 429 (1964).
[42] M. Ross and H. B. Radousky, Phys. Lett. A **129**, 43 (1988).
[43] W. Hogevorst, Physica **51**, 59 (1971).
[44] N. Schwentner, E. E. Koch, and J. Jortner, *Electronic Excitations in Condensed Rare Gases* (Springer, Heidelberg, 1985).
[45] M. Ross, W. J. Nellis, and A. C. Mitchell, Chem. Phys. Lett. **68**, 532 (1979).
[46] W. J. Nellis and A. C. Mitchell, J. Chem. Phys. **73**, 6137 (1980).
[47] M. Ross and F. H. Ree, J. Chem. Phys. **73**, 6146 (1980).
[48] M. Ross, F. H. Ree, and D. A. Young, J. Chem. Phys. **79**, 1487 (1983).
[49] M. Ross, H. K. Mao, P. M. Bell, and J. A. Xu, J. Chem. Phys. **85**, 1028 (1986).
[50] H. B. Radousky and M. Ross, in *Simple Molecular Systems at Very High Density*, edited by A. Polian, P. Loubeyre, and N. Boccara (Plenum, New York, 1989).
[51] L. D. Landau and E. M. Lifshitz, *Fluid Mechanics* (Pergamon, Oxford, 1963).
[52] J. M. Eisenberg and W. Greiner, *Nuclear Models* (North–Holland, Amsterdam, 1987).
[53] W. Schmidt, U. Katscher, B. Waldhauser, J. A. Maruhn, H. Stöcker, and W. Greiner, in *The Nuclear Equation of State, Part A: Discovery of Nuclear Shock Waves and the EOS*, edited by W. Greiner and H. Stöcker (Plenum, New York, 1989).